MRS Communications (2021) 11:100–105

https://doi.org/10.1557/s43579-020-00005-9

MRS Communications

Polymers for Additive Manufacturing Research Letter

Mechanical and thermal properties of 3D-printed epoxy composites reinforced with boron nitride nanobarbs

Brett G. Compton, Mechanical, Aerospace, and Biomedical Engineering Department, University of Tennessee, Knoxville, TN 37996, USA; Materials Science and Engineering Department, University of Tennessee, Knoxville, TN 37996, USA
Jackson K. Wilt, James W. Kemp, and **Nadim S. Hmeidat,** Mechanical, Aerospace, and Biomedical Engineering Department, University of Tennessee, Knoxville, TN 37996, USA
Samantha R. Maness, Materials Science and Engineering Department, University of Tennessee, Knoxville, TN 37996, USA
Mark Edmond, Steve Wilcenski, and **Jason Taylor,** BNNano, Cary, NC 27519, USA

Address all correspondence to Brett G. Compton at **brettcompton@utk.edu**

(Received 23 September 2020; accepted 9 December 2020; published online 19 January 2021)

Abstract

In this work, new boron nitride-reinforced epoxy-based composite inks for direct-ink write (DIW) additive manufacturing are presented. Printed composites are characterized for thermal conductivity, flexure, and impact energy, along with optical and electron microscopy. The new inks utilize boron nitride nanobarbs (BNNBs), a novel form of boron nitride nanotube, where the surface is decorated with hexagonal boron nitride nanoplatelets. BNNBs are shown to improve the thermal conductivity of the printed composites up to 32%, the strength up to 34%, and stiffness up to 44%. Anisotropy was observed in all measurements, suggesting that the BNNBs become aligned during printing.

Introduction

Boron nitride nanotubes (BNNTs) are a one-dimensional nanoscale material analogous to carbon nanotubes (CNTs) but consisting of boron and nitrogen atoms instead of carbon. Like CNTs, BNNTs are ~10–50 nm in diameter, up to tens of microns in length, can be single- or multi-walled, and have superior mechanical properties, demonstrating Young's modulus of up to 1.3 TPa,[1] tensile strength up to 33 GPa,[1] and thermal conductivity up to 2400 W/m/K.[2] In addition, BNNTs have a higher oxidation resistance than CNTs and are stable in air up to 850°C vs 500°C for CNTs.[3] BNNTs are also electrically resistive with a band gap of ~5.5 eV[4] and dielectric constant of 5.9.[5]

CNT use as a reinforcement in composite materials has been somewhat limited by (i) agglomerations due to van der Waals forces limiting the amount that may be uniformly dispersed within a matrix and (ii) weak interfacial interaction between the CNTs and polymer matrix candidates.[6] In contrast, BNNTs display both superior wettability and dispersion when added to epoxy resins.[6] In addition, the polarity of B–N bonds[7] produces stronger matrix interfacial interactions that ultimately result in higher mechanical performance at comparable loadings, as well as the ability to add larger total amounts without agglomeration.[6]

Recent developments in chemical surface modifications to CNTs have enabled their more widespread use as a reinforcement in polymer composites due to reductions in agglomeration and increases in polymer matrix interfacial bonding strength. Similar improvements have been proposed for BNNTs,[8] but developments in this area lag behind that of CNTs. However, in addition to chemical modification, nanotube morphological modification has the potential to reduce agglomeration and increase interaction with polymer matrices, thereby increasing the efficacy of BNNTs as mechanical reinforcement. For example, boron nitride NanoBarbs™ (BNNBs) are BNNTs that have been enhanced through surface nucleation of hexagonal boron nitride (hBN) crystals (Fig. 1a). The hBN dispersed along the BNNT creates an irregular surface which serves to limit agglomeration by maintaining sufficient distances between surfaces, thereby reducing van der Waals attraction between nanotubes. In addition, hBN decoration serves to increase matrix interfacial interaction by permitting mechanical interlocking between the BNNT surface and matrix while maintaining B–N polarity.

Recently, additive manufacturing (AM) methods have demonstrated considerable opportunities to fabricate composite and hybrid materials with unique mesostructural and microstructural architecture, including control over the arrangement and orientation of high-aspect ratio filler materials.[9–17] Material extrusion AM presents unique capabilities for such control due to the fact that the shear flow phenomenon associated with extrusion tends to align high-aspect ratio fillers. For example, Shofner et al. showed that CNTs align in the print direction during printing of CNT-reinforced ABS thermoplastic, leading to improved strength and modulus along the print direction.[17] More recently, Hmeidat et al. demonstrated that the material extrusion AM process effectively orients nanoclay platelets and silicon carbide (SiC) microfibers along the print direction, with

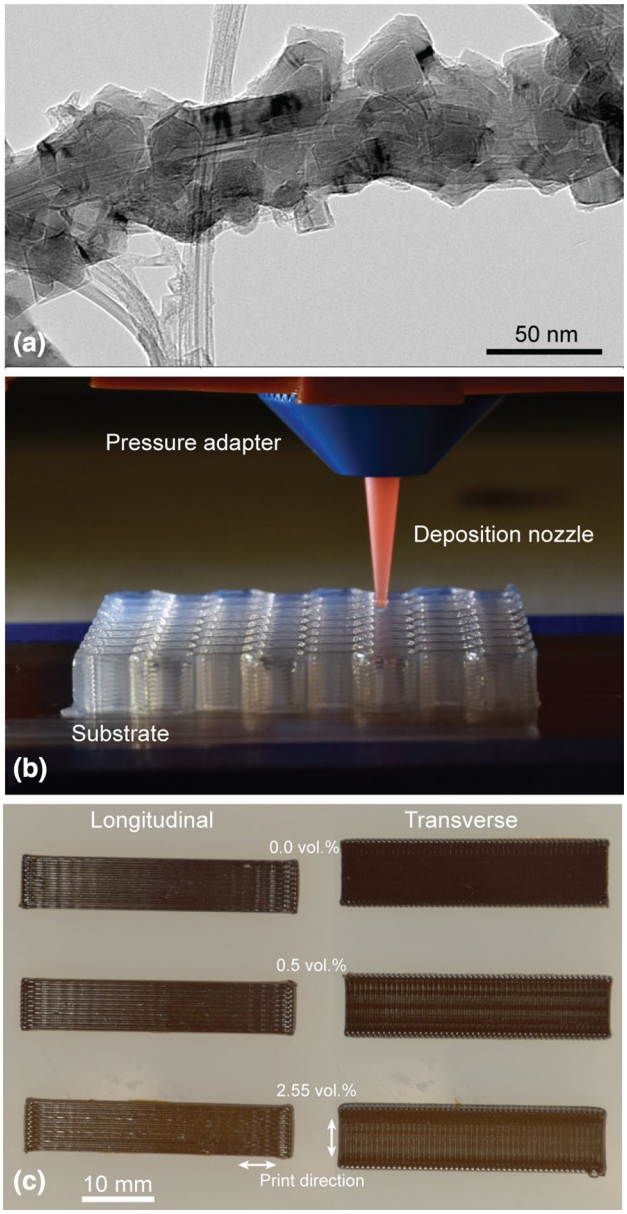

Figure 1. (a) Transmission electron microscopy (TEM) image of a decorated boron nitride nanobarb. Image courtesy of BNnano. (b) The direct-ink write 3D printing platform with printed silicone honeycomb. (c) Printed 3-pt flexure bars for the present study.

the use of smaller deposition nozzles and higher printing speeds leading to increased filler alignment, resulting in higher mechanical anisotropy.[12, 18] The alignment of the microfibers was confirmed with scanning electron microscopy (SEM), while the orientation of nanoclay platelets was measured using small-angle X-ray-scattering (SAXS). In this work, researchers also found that reinforcement with fumed silica, comprised of spheroidal silica nanoparticles, did not result in any measurable mechanical anisotropy within the printed epoxy composites.[12]

Transport properties in printed polymer composites have received somewhat less attention than mechanical properties, but recent work has shown considerable promise. For example, Collino et al. demonstrated that acoustic fields can be used to spatially partition multiple filler materials in epoxy resin during a printing process,[9, 10] and Melchert et al. used acoustic fields to arrange and orient conductive carbon fibers in a flexible polymer matrix to control anisotropic conductivity.[14] Kokkinis demonstrated elegant control over composition and orientation of magnetically functionalized alumina platelets in a polymer matrix through selective application and manipulation of magnetic fields during the printing and curing process.[19] Raney and Compton et al. achieved unique helical arrangements of carbon fibers in a 3D-printed epoxy composite by rotating the material extrusion print head during the printing process.[15] In this process, the ratio of rotation rate to translation rate influences the helical angle of fibers relative to the filament axis and enables some portion of fibers to be reoriented transverse to the layer plane. Such developments present new opportunities to improve functionality of printed components by controlling and designing the orientation of thermally conductive filler materials in 3D printing feedstocks.

Here, we report the mechanical and thermal properties of new 3D-printed boron nitride nanobarb/epoxy composites that show exceptional property improvement with small additions of BNNBs. The deposition process is shown to impart thermal and mechanical anisotropy to the printed composites which is attributed to the orientation of the BNNBs. Results highlight the promise of small additions of BNNBs to existing epoxy composite ink formulations to further improve strength, stiffness, and thermal properties.

Experimental

DIW inks were formulated using Epon 826 epoxy resin (Hexion, Inc., Columbus, OH), with Cab-o-sil TS-720 fumed silica (Cabot Corporation, Alpharetta, GA) as the viscosifying additive. This particular fumed silica is functionalized with polydimethylsiloxane (PDMS) and has a base surface area of 200 m^2/g (www.cabotcorp.com/solutions/products-plus/fumed-metal-oxides/hydrophilic). Primary particle size is typically ~ 7–40 nm.[20] 1-ethyl-3-methylimidazolium dicyanamide (EMIM DCA) ionic liquid was used as the latent curing agent (BASF Basionics VS 03, obtained from Sigma Aldrich, Inc., St. Louis, MO). BNNBs (BNNano, Cary, NC) were first dispersed in the epoxy resin via high-shear mixing to result in mixtures containing 1 wt% and 5 wt% BNNBs. The BNNBs have nominal length of 10 μm, nominal diameter of 8 nm, and nominal hBN decoration ~ 25 nm in thickness (BNnano, private communication). To the epoxy/BNNB mixtures, 11.11 parts per hundred (pph) fumed silica and 5 pph curing agent (relative to the mass of the epoxy resin) were added sequentially, with each addition of material followed by mixing in a centrifugal planetary mixer (FlackTek, Inc., Landrum, SC) at 1700 rpm and 100 Torr (133.3 kPa) for 4 minutes. An additional baseline ink was also formulated without any BNNBs for comparison. The mixing procedure follows that described in Hmeidat et al.[18]

and resulted in bubble-free, printable inks. The final ink formulations contained 0 vol.%, 0.5 vol.%, and 2.55 vol.% BNNBs, which will be subsequently referred to as 0BN, 0.5BN, and 2.5BN, respectively.

Following mixing, inks were loaded by spatula into 10 cm^3 syringe barrels which were capped and centrifuged at 4000 rpm for 7 min (Sorvall™ ST-8 Centrifuge, Thermo Fisher Scientific, Waltham, MA) to remove air pockets in the ink that may have been introduced during loading. Loaded syringe barrels were then placed in a high-pressure adaptor (HP3, Nordson EFD, Westlake, OH), mounted on a 3-axis positioning stage (Shopbot Tools, Inc., Durham, NC), and connected to a voltage-controlled pressure regulator (Omega Engineering, Inc., Norwalk, CT) to extrude the material pneumatically. Print paths were generated in G-code using Scilab software (Scilab Enterprises, France) and all samples were printed at 30 mm/s using a 577-µm-diameter tapered Luer-lock nozzle tip (McMaster-Carr, Elmhurst, IL). Build plates were coated with adhesive-backed PTFE-coated aluminum foil (Bytac, Saint Gobain North America, Malvern, PA) to prevent permanent adhesion, following Compton and Lewis.[11] The printing platform is shown in Fig. 1b. Rectangular bars were printed and cured for thermal conductivity measurements, flexural tests, and Izod impact testing. Thermal conductivity samples were cut from large printed bars using a low-speed diamond saw (Allied High Tech) and thermal conductivity measurements were made using the transient plane source method[21] (TPS 2500 S, ThermTest USA, Charlottesville, VA). For each formulation, two sets of thermal conductivity measurements were made, one with the print direction oriented normal to the planar source (orientation 1), and one with the print direction oriented parallel to the planar source (orientation 2). Flexural tests were conducted at room temperature by means of an electromechanical load frame (Model 45, MTS Systems Corporation, Eden Prairie, MN, USA), equipped with a 10 kN load cell. Specimens with nominal dimensions of ~40 mm × 8 mm × 2 mm were tested in 3 -pt flexure using a crosshead rate of 0.9 mm/min and span length of 32 mm. Two sets of bars were printed with unidirectional print paths, one oriented along the length of the bend bar (longitudinal), and one oriented transverse to the length of the bend bar (transverse) (Fig. 1c). At least three specimens were tested for each formulation and print direction. Additional rectangular samples were printed for Izod impact testing with nominal dimensions of 65 mm × 12.5 mm × 6 mm. All Izod samples were printed with the print path oriented along the long dimension of the bar, and after printing, samples were milled and notched for testing in accordance with ASTM D256-10(2018). At least four impact tests were conducted for each formulation.

Results and discussion

Printed objects are shown in Fig. 1c. All three formulations printed successfully and the presence of BNNBs was not observed to substantially change the printing behavior. That is, the inks containing BNNBs were able to be printed using the same nozzle size and print speed as the 0BN ink without clogging or introducing obvious defects to the printed samples. Thermal conductivity was found to increase with the presence of BNNBs for both orientations tested, from 0.236 W/m K for the 0BN ink in both orientations to 0.27 W/m K and 0.31 W/m K in orientation 1 for the 0.5BN and 2.5BN inks, respectively, and to 0.245 W/m K and 0.283 W/m K in orientation 2 for the 0.5BN and 2.5BN inks, respectively (Fig. 2a). When tested in orientation 1, these values represent in an increase in thermal conductivity of 14.7% and 31.6% over the base material, while measurements in orientation 2 are only 3.8% and 19.6%

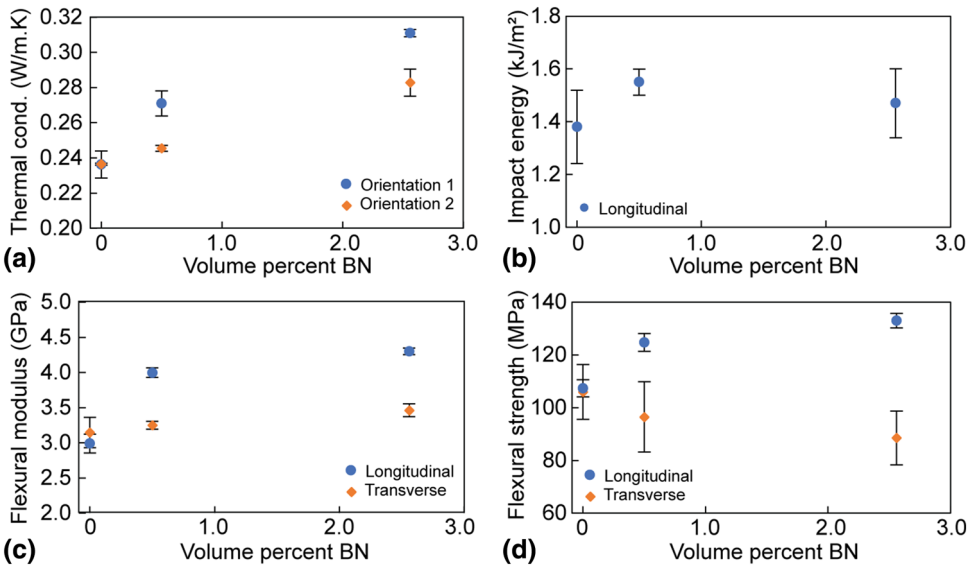

Figure 2. (a) Thermal conductivity of the printed composite measured in two orthogonal orientations. (b) Izod impact energy of the printed composite measured along the print direction. (c) Flexural modulus of the printed composites measured along and transverse to the print direction. (d) Flexural strength of the printed composites.

higher than the base material, for the 0.5BN and 2.5BN inks, respectively. The differences in thermal conductivity observed between orientations may be a result of printing-induced orientation of the BNNBs, but it should be noted that these specific plane source measurements were made in isotropic mode; the true thermal conductivity along each material direction remains unknown and will be the focus of a dedicated follow-on study.

Izod impact data are shown in Fig. 2b. The impact energy of the base material is 1.38 ± 0.139 kJ/m^2, while the 0.5BN composite displayed an impact energy of 1.55 ± 0.049 kJ/m^2 and the 2.5BN composite was measured as 1.47 ± 0.131 kJ/m^2. Although the mean values show some improvement in impact energy with BNNBs, the standard deviation in measurements is quite large and an analysis of variance indicated that the individual datasets are not significantly different.

The flexural modulus and strength for all the printed composites are plotted in Fig. 2c, d. For the longitudinal specimens, the flexural modulus increased from 2.99 ± 0.13 to 4.0 ± 0.07 GPa (a 34% increase) for the 0.5BN composite, and to 4.3 GPa (a 44% increase) for the 2.5BN composite. Conversely, for the transverse specimens, the modulus did not significantly change with the addition of 0.5 vol.% BN (3.15 ± 0.22 GPa for 0BN compared to 3.25 ± 0.06 GPa for the 0.5BN composite), and only increased moderately to 3.46 ± 0.09 GPa (a 10% increase) for the 2.5BN composite. Flexural strength values were observed to increase monotonically with increasing BN loading in the longitudinal specimens, whereas a mild decrease in strength was observed in the transverse specimens with increasing BN loading. Specifically, along the print direction, strength increases from 107.3 ± 3.2 MPa to 124.8 ± 3.3 and $133.0 \pm 0.2.7$ MPa for the 0.5BN and 2.5BN composites, respectively, corresponding to a 16% and 24% increase. Transverse to the print direction, strength decreases from 106.0 ± 10.4 MPa to 96.5 ± 13.3 and 88.5 ± 10.2 MPa for the 0.5BN and 2.5BN composites, respectively, corresponding to a 9% and 16.5% decrease. Hmeidat et al.[12] studied the same base composite reinforced with fumed silica and found no dependence of flexural strength or stiffness on the print direction, nozzle size, or print speed. Based on Hmeidat's results, the anisotropy observed in the present study is attributed to the alignment of the BNNBs during the printing process.

Optical micrographs of the fracture surfaces of the longitudinal flexure specimens show the characteristic mirror, mist, and hackle regions indicative of brittle fracture in glassy polymers (Fig. 3a, c, e).[22, 23] For the 0BN and 0.5BN composites, a small subsurface flaw is visible in the mirror region that likely acted as the crack initiation point, while no such flaw is immediately apparent in the 2.5BN composite. The fact that the flaws are subsurface for the former two samples provide confidence that the surface texture that results from the printing process was not a major strength-limiting feature. As BN content increases, the roughness of the fracture surfaces increases as well, which may be indicative of the BNNBs acting as crack deflection points during crack growth. Fracture surfaces also show that the flexural bars are devoid of large, printing-related pores. Optical micrographs of the fracture surfaces of the Izod impact test specimens are shown in Fig. 3b, d, f. In contrast to the flexural specimens, the Izod fracture surfaces are predominantly smooth and glassy for all three formulations. The machined notch can be seen on the right side of each sample, but the 0BN and 0.5BN

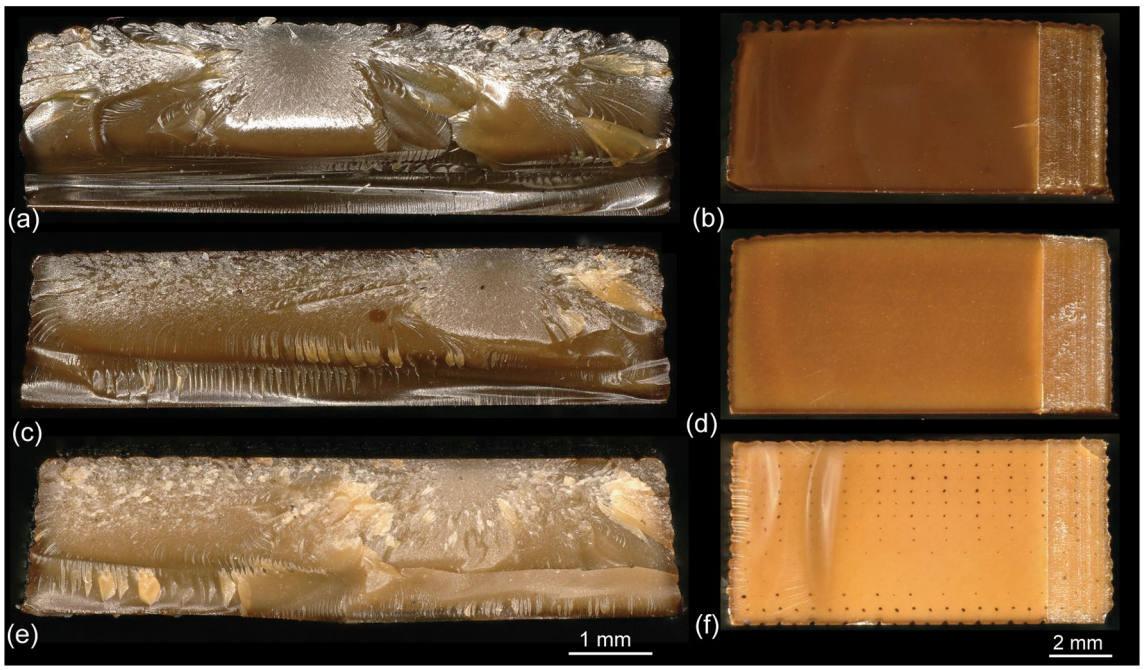

Figure 3. (a), (c), (e) Optical micrographs of the fracture surfaces of 3-pt flexure specimens. (b), (d), (f) Optical micrographs of the fracture surfaces of Izod impact specimens. (a), (b) 0BN composite. (c), (d) 0.5BN composite. (e), (f) 2.5BN composite.

composites are otherwise free of distinguishing features. The 2.5BN composite contains a regular array of small, dark features that have spacing equivalent to the spacing between printed filaments. While these features may appear to be interstitial void spaces between filaments, as has been regularly documented in thermoplastic material extrusion methods,[24–26] they are not actually voids. Close inspection of the fracture surface revealed that all of the dark features are filled with cured epoxy resin that does not appear to contain either of the filler materials. Hmeidat et al.[18] observed similar features in printed epoxy/nanoclay composites. In that work, they suggested that the epoxy resin may seep out of the filler network during the curing process to "heal" small voids in the microstructure.

High-magnification scanning electron microscopy (SEM) images of the fracture surfaces of the 2.5BN flexural samples are shown in Fig. 4. Individual nanobarbs are visible on the surface of both the longitudinal specimens (Fig. 4a) and the transverse specimens (Fig. 4b). Some of the exposed BNNBs are highlighted on the images with yellow ellipses and boxes, but many others can be seen on the surfaces as well. Based on the projected area and the relative frequency of the BNNBs, some degree of orientation with printing direction is apparent, with more frequent, but shorter segments visible on the longitudinal sample than on the transverse sample. For the same volume fraction, a higher number of visible barbs would be expected on a section plane transverse to the orientation of the barbs through a simple probability argument as discussed by Bay and Tucker III[27] in the context of fiber orientation tensors. Although this is not definitive proof of a high degree of orientation, these qualitative observations corroborate the anisotropic elastic modulus and flexural strength measurements in these printed composites.

Although dispersion of the BNNBs appears to be good in most cases, some agglomerations of fumed silica and BNNBs are apparent on the fracture surfaces. One such example is shown in Fig. 4c, where several long BNNBs can be seen bridging a void in the epoxy matrix on the fracture surface of a longitudinal flexure specimen. Interestingly, the individual BNNBs appear to be well-separated from one another despite the higher concentration in this region. The barbs are several microns in length, with the longest having approximately seven microns exposed with each end embedded in the epoxy matrix. A higher number of these agglomerations were observed in the 2.5BN samples compared to the 0.5BN samples, which may explain the diminishing returns in thermal and mechanical property improvement with the addition of 2.55 vol.% BNNBs compared with the addition of only 0.5 vol.% BNNBs. Finally, the agglomerates that were observed on fracture surfaces were generally comprised of both fumed silica agglomerates and BNNB agglomerates, suggesting that there may be interaction between the two species whereby a preexisting fumed silica agglomerate may attract or collect the longer BNNBs in the mixture or vice versa. Similar potential interaction between fumed silica and silicon carbide microfibers has been discussed by Hmeidat et al.,[12] and this will be an important area for future study to

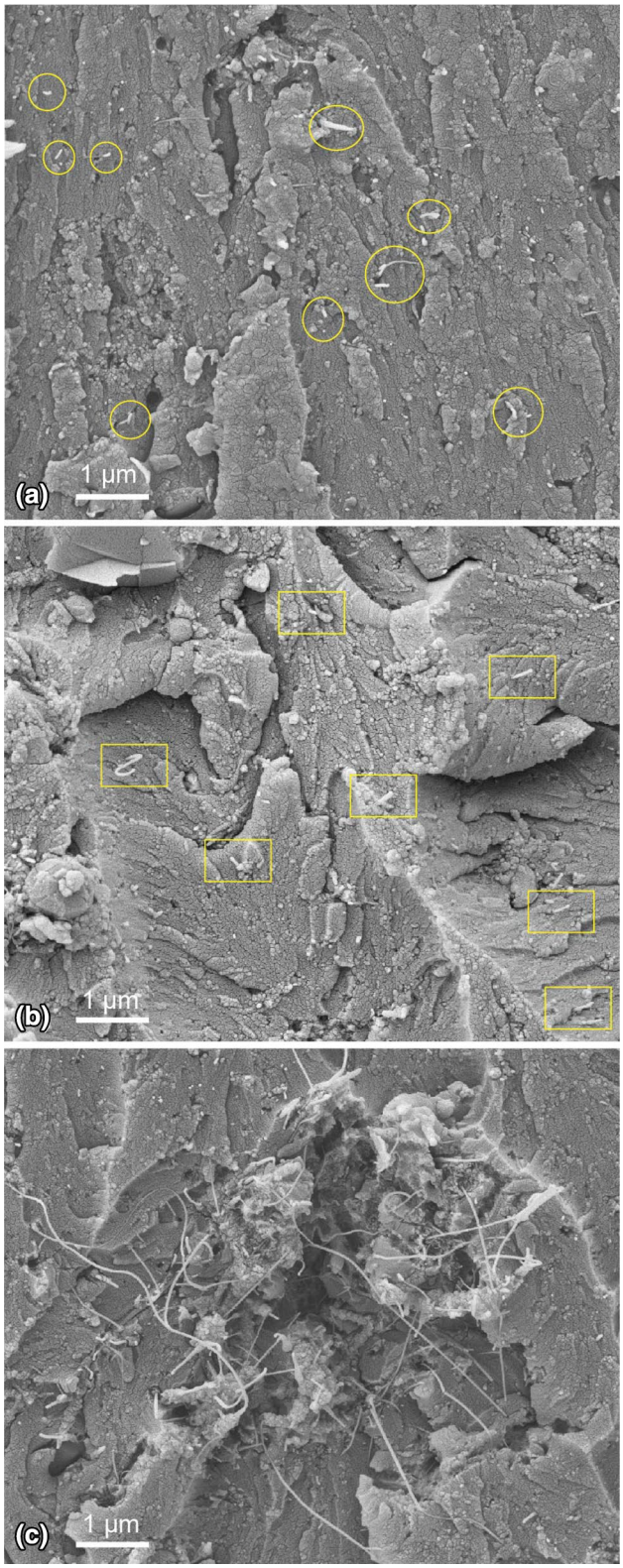

Figure 4. SEM images of the fracture surfaces of 3-pt flexure specimens. (a) Longitudinal sample. Some BNNBs are indicated by yellow ellipses. (b) Transverse sample. Some BNNBs are highlighted with yellow boxes. (c) An agglomerate of fumed silica and long BNNBs observed in the longitudinal sample.

enable the refinement and improvement of multi-component epoxy-based DIW inks.

Summary and conclusion

In summary, novel epoxy-based DIW inks have been formulated with Epon 826 resin, fumed silica, and 0.5 or 2.55 vol.% BNNBs. Thermal conductivity was enhanced up to 32% with the addition of BNNBs, while flexural modulus was enhanced up to 44% and flexural strength up to 24% at the highest loading tested. Impact energy was not strongly affected with the addition of BNNBs. All printed composites containing BNNBs displayed anisotropy that is characteristic of 3D-printed composite materials, with greater property improvements occurring along the print direction due to the alignment of the reinforcing phases. Microscopy of fracture surfaces revealed predominantly pore-free printed composites with corroborating evidence of BNNB alignment along the print direction and the presence of some agglomerates containing BNNBs several microns long. The work suggests high potential for BNNBs as low-volume fraction constituents in high-performance, multifunctional epoxy-based 3D-printed composites.

Acknowledgments

This work was generously supported by Honeywell Federal Manufacturing and Technologies through Contract DE-NA0002839. BGC, JKW, NSH, and SRM would also like to acknowledge support from the Tennessee Higher Education Commission (THEC) Center for Materials Processing (CMP), and JWK would like to acknowledge support from the University of Tennessee Chancellor's Fellowship. BNNBs were generously provided by BNNano.

Compliance with ethical standards

Conflict of interest

Steve Wilcenski, Mark Edmond, and Jason Taylor have financial interest in BNNano, who supplied the boron nitride nanobarbs for this study. All other authors have no financial interests to declare.

References

1. X. Wei, M.S. Wang, Y. Bando, D. Golberg, Tensile tests on individual multi-walled boron nitride nanotubes. *Adv. Mater.* **22**(43), 4895–4899 (2010)
2. B.E. Belkerk, A. Achour, D. Zhang, S. Sahli, M.-A. Djouadi, Y.K. Yap, Thermal conductivity of vertically aligned boron nitride nanotubes. *Appl. Phys. Express* **9**(7), 075002 (2016)
3. C. Zhi, Y. Bando, C. Tang, D. Golberg, Boron nitride nanotubes. *Mater. Sci. Eng. R* **70**(3–6), 92–111 (2010)
4. X. Blase, A. Rubio, S. Louie, M. Cohen, Stability and band gap constancy of boron nitride nanotubes. *Europhys. Lett.* **28**(5), 335 (1994)
5. H.-P. Lan, L.-H. Ye, S. Zhang, L.-M. Peng, Transverse dielectric properties of boron nitride nanotubes by ab initio electric field calculations. *Appl. Phys. Lett.* **94**(18), 183110 (2009)
6. J. Guan, B. Ashrafi, Y. Martinez-Rubi, M.B. Jakubinek, M. Rahmat, K.S. Kim, B. Simard, Epoxy resin nanocomposites with hydroxyl (OH) and amino (NH_2) functionalized boron nitride nanotubes. *Nanocomposites* **4**(1), 10–17 (2018)
7. X. Chen, L. Zhang, C. Park, C.C. Fay, X. Wang, C. Ke, Mechanical strength of boron nitride nanotube–polymer interfaces. *Appl. Phys. Lett.* **107**(25), 253105 (2015)
8. C. Zhi, Y. Bando, C. Tang, Q. Huang, D. Golberg, Boron nitride nanotubes: functionalization and composites. *J. Mater. Chem.* **18**(33), 3900–3908 (2008)
9. R.R. Collino, T.R. Ray, R.C. Fleming, J.D. Cornell, B.G. Compton, M.R. Begley, Deposition of ordered two-phase materials using microfluidic print nozzles with acoustic focusing. *Extreme Mech. Lett.* **8**, 96–106 (2016). https://doi.org/10.1016/j.eml.2016.04.003
10. R.R. Collino, T.R. Ray, R.C. Fleming, C.H. Sasaki, H. Haj-Hariri, M.R. Begley, Acoustic field controlled patterning and assembly of anisotropic particles. *Extreme Mech. Lett.* **5**, 37–46 (2015)
11. B.G. Compton, J.A. Lewis, 3D-printing of lightweight cellular composites. *Adv. Mater.* **26**(34), 5930–5935 (2014). https://doi.org/10.1002/adma.201401804
12. N.S. Hmeidat, R.C. Pack, S.J. Talley, R.B. Moore, B.G. Compton, Mechanical anisotropy in polymer composites produced by material extrusion additive manufacturing. *Addit. Manuf.* **34**, 101385 (2020). https://doi.org/10.1016/j.addma.2020.101385
13. J.P. Lewicki, J.N. Rodriguez, C. Zhu, M.A. Worsley, A.S. Wu, Y. Kanarska, J.D. Horn, E.B. Duoss, J.M. Ortega, W. Elmer, 3D-printing of meso-structurally ordered carbon fiber/polymer composites with unprecedented orthotropic physical properties. *Sci. Rep.* **7**, 43401 (2017)
14. D.S. Melchert, R.R. Collino, T.R. Ray, N.D. Dolinski, L. Friedrich, M.R. Begley, D.S. Gianola, Flexible conductive composites with programmed electrical anisotropy using acoustophoresis. *Adv. Mater. Technol.* **4**(12), 1900586 (2019)
15. J.R. Raney, B.G. Compton, J. Mueller, T.J. Ober, K. Shea, J.A. Lewis, Rotational 3D printing of damage-tolerant composites with programmable mechanics. *Proc. Natl Acad. Sci. USA* **115**(6), 1198–1203 (2018). https://doi.org/10.1073/pnas.1715157115
16. C. Shemelya, A. De La Rosa, A.R. Torrado, K. Yu, J. Domanowski, P.J. Bonacuse, R.E. Martin, M. Juhasz, F. Hurwitz, R.B. Wicker, Anisotropy of thermal conductivity in 3D printed polymer matrix composites for space based cube satellites. *Addit. Manuf.* **16**, 186–196 (2017)
17. M. Shofner, K. Lozano, F. Rodríguez-Macías, E. Barrera, Nanofiber-reinforced polymers prepared by fused deposition modeling. *J. Appl. Polym. Sci.* **89**(11), 3081–3090 (2003)
18. N.S. Hmeidat, J.W. Kemp, B.G. Compton, High-strength epoxy nanocomposites for 3D printing. *Compos. Sci. Technol.* **160**, 9–20 (2018). https://doi.org/10.1016/j.compscitech.2018.03.008
19. D. Kokkinis, M. Schaffner, A.R. Studart, Multimaterial magnetically assisted 3D printing of composite materials. *Nat. Commun.* (2015). https://doi.org/10.1038/ncomms9643
20. A.L. Andrady, T.C. Merkel, L.G. Toy, Effect of particle size on gas permeability of filled superglassy polymers. *Macromolecules* **37**(11), 4329–4331 (2004)
21. S.E. Gustafsson, Transient plane source techniques for thermal conductivity and thermal diffusivity measurements of solid materials. *Rev. Sci. Instrum.* **62**(3), 797–804 (1991)
22. W. Cantwell, A. Roulin-Moloney, T. Kaiser, Fractography of unfilled and particulate-filled epoxy resins. *J. Mater. Sci.* **23**(5), 1615–1631 (1988)
23. L. Plangsangmas, J.J. Mecholsky Jr., A.B. Brennan, Determination of fracture toughness of epoxy using fractography. *J. Appl. Polym. Sci.* **72**(2), 257–268 (1999)
24. S.H. Ahn, M. Montero, D. Odell, S. Roundy, P.K. Wright, Anisotropic material properties of fused deposition modeling ABS. *Rapid Prototyp. J.* **8**(4), 248–257 (2002). https://doi.org/10.1108/13552540210441166
25. C.E. Duty, V. Kunc, B. Compton, B. Post, D. Erdman, R. Smith, R. Lind, P. Lloyd, L. Love, Structure and mechanical behavior of Big Area Additive Manufacturing (BAAM) materials. *Rapid Prototyp. J.* **23**(1), 181–189 (2017)
26. H.L. Tekinalp, V. Kunc, G.M. Velez-Garcia, C.E. Duty, L.J. Love, A.K. Naskar, C.A. Blue, S. Ozcan, Highly oriented carbon fiber-polymer composites via additive manufacturing. *Compos. Sci. Technol.* **105**, 144–150 (2014). https://doi.org/10.1016/j.compscitech.2014.10.009
27. R.S. Bay, C.L. Tucker III., Stereological measurement and error estimates for three-dimensional fiber orientation. *Polym. Eng. Sci.* **32**(4), 240–253 (1992)